ACS Catalysis

Research Article

Cite This: ACS Catal. 2019, 9, 5391−5399

pubs.acs.org/acscatalysis

Enzymatic Pyran Formation Involved in Xiamenmycin Biosynthesis

Bei-Bei He,[†,‡] Ting Zhou,[‡] Xu-Liang Bu,[‡] Jing-Yi Weng,[†] Jun Xu,[‡,§] Shuangjun Lin,[‡] Jian-Ting Zheng,*[,‡] Yi-Lei Zhao,*[,‡] and Min-Juan Xu*[,†]

[†]Key Laboratory of Systems Biomedicine (Ministry of Education), Shanghai Center for Systems Biomedicine, Shanghai Jiao Tong University, Shanghai 200240, People's Republic of China

[‡]State Key Laboratory of Microbial Metabolism, School of Life Sciences and Biotechnology, Shanghai Jiao Tong University, Shanghai 200240, People's Republic of China

[§]School of Oceanography, Shanghai Jiao Tong University, Shanghai 200240, People's Republic of China

Supporting Information

ABSTRACT: The pyran ring is a very common structural unit of many natural, bioactive molecules that are widely found in plants, bacteria, and fungi. However, the enzymatic processes by which many of these pyran-containing molecules are formed are unclear. Herein, we report the construction of the pyran ring catalyzed by the cooperation of a flavin-dependent monooxygenase, XimD, and a SnoaL-like cyclase, XimE, in the biosynthesis of xiamenmycins. XimD catalyzes the formation of an epoxide intermediate that spontaneously transforms to furan and pyran products (43:1) in vitro. XimE then catalyzes the formation of the pyran ring in a 6-endo configuration from the epoxide to yield a benzopyran, xiamenmycin B. Further, we obtained the crystallographic structure of XimE, with and without product, which suggests a synergistic mechanism in which a group of four residues (Y46−Y90−H102−E136) acts cooperatively as the general acid and base. Subsequent structure-based analysis of possible viable substrates indicates that both XimD and XimE exhibit high promiscuity in their catalysis. Overall, this study reveals the mechanism of pyran ring formation in xiamenmycin biosynthesis and demonstrates the potential application of XimD and XimE in the biosynthesis of other benzoheterocycle scaffolds, including furano- and pyranocoumarins.

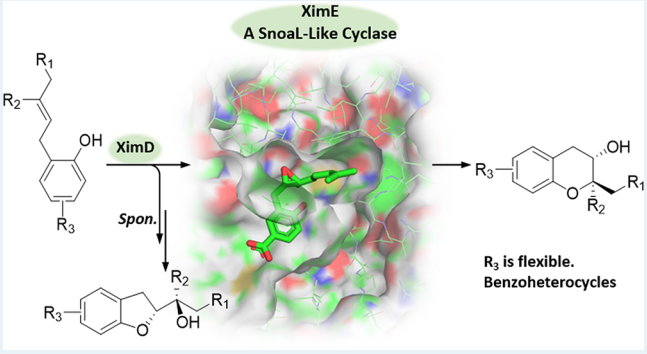

KEYWORDS: *SnoaL-like cyclase, benzopyran, catalytic promiscuity, reaction mechanism, biosynthesis*

INTRODUCTION

The tetrahydropyran ring is a common structural feature of many natural bioactive molecules. Notable examples include bacterial polyketides,[1−4] such as lasalocid A, monensin, and salinomycin, the fungal polyketide aurovertins,[5] and plant chromenes, such as tetrahydrocannabinolic acid.[6,7] The pyran ring within these compounds is usually formed via (i) epoxidation of an olefin substrate followed by epoxide hydrolase catalyzed epoxide ring opening reactions,[5,8] (ii) a berberine bridge enzyme catalyzed hydride transfer reaction,[6,9] or (iii) a pyran synthase catalyzed oxa-Michael addition.[10,11] The sophistication of the processes by which these natural products are biosynthesized in vivo suggests that the corresponding enzymes have been highly optimized for the formation of the pyran skeleton.

A pyran ring containing scaffold that has recently begun to attract increased attention is 3-chromanol.[12−14] This is a relatively common skeleton found in a wide range of bioactive molecules from plants and microbial species, including the antibacterial kuhistanol D from *Ferula kuhistanica*,[15,16] the anticancer pyranocoumarin decursin from *Angelica gigas*,[17] and the xiamenmycins from *Streptomyces xiamenensis* 318 (Figure 1 and Figure S1).[18,19] Of note with the last species, the carboxyl group in xiamenmycin B (**1**) undergoes a substitution reaction to produce various potent bioactive homologues, such as the L-threonine amidated derivative xiamenmycin A, which exhibits antifibrotic and anti-inflammatory activities.[19] However, despite its wide distribution and frequent occurrence, the enzymatic process by which the 3-chromanol skeleton is produced in any of these molecules has not yet been elucidated.

Nonetheless, great efforts have been made to obtain this promising pharmacophore. The chemical synthesis processes of 3-chromanols have been intensively investigated,[12,13,20−25] including Au-catalyzed intramolecular cycloalkylation,[13] $FeBr_3$/3AgOTf-mediated cyclization of aryl glycidyl ether,[12] and $VO(acac)_2$/TBHP catalyzed oxidative cyclization.[24] Biologists tried to produce bioactive 3-chromanol-containing derivatives via *Mycobacterium* biotransformation[26] and engineered the metabolic pathway to improve the production of

Received: March 11, 2019
Revised: April 21, 2019
Published: May 2, 2019

DOI: 10.1021/acscatal.9b01034
ACS Catal. 2019, 9, 5391−5399

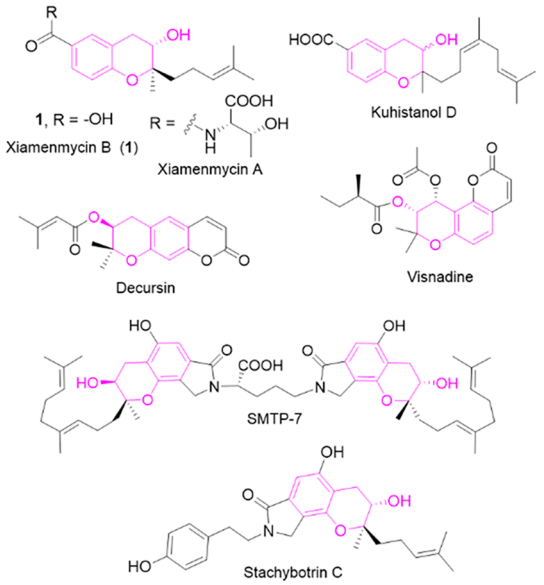

Figure 1. Examples of bioactive natural products and drugs containing the 3-chromanol skeleton (highlighted in purple). Visnadine is a vasodilator drug, isolated from *Ammi visnaga*.[29] SMTP-7 is a thrombolytic stroke drug, isolated from *Stachybotrys microspora*.[30,31] Stachybotrin C exhibits neuroprotective activity, isolated from *Stachybotrys parvispor*.[32]

pyranocoumarins in native plant hosts.[27,28] An environmentally friendly, renewable, and sustainable strategy to produce this widely spread bioactive skeleton is still unavailable. Thus, discovering and understanding the specific enzymes that can generate the 3-chromanol building block under mild conditions is expected to significantly enhance our abilities to more effectively produce the aforementioned bioactive compounds as well as develop novel derivatives thereof.

Here, we describe the mechanism of 3-chromanol ring formation in the biosynthetic pathway of xiamenmycin and report the apo and cocrystal X-ray structures of the key SnoaL-like cyclase XimE, which regioselectively catalyzes the formation of a C^2–O bond to generate the 3-chromanol skeleton. By site-directed mutagenesis and computational studies, we identify the key residues that govern the regioselectivity in this XimE and, on the basis of the cocrystal structure, rationally expand the substrate repertoire of this enzyme. Together with its upstream flavin-dependent monooxygenase (FMO) XimD, we show that these two enzymes are capable of producing 14 products with 6 different benzoheterocycle scaffolds.

RESULTS AND DISCUSSION

Role of FMO and a SnoaL-like Cyclase in Xiamenmycin Biosynthesis. The xiamenmycin biosynthetic gene cluster was previously identified to consist of five genes (Figure 2A).[19] This earlier work demonstrated that the initial step in this pathway is mediated by XimC, a chorismate lyase (*ximC*), that cleaves chorismate to produce 4-hydroxybenzoate (4-HBA), which is then prenylated by 4-HBA prenyltransferase (*ximB*)

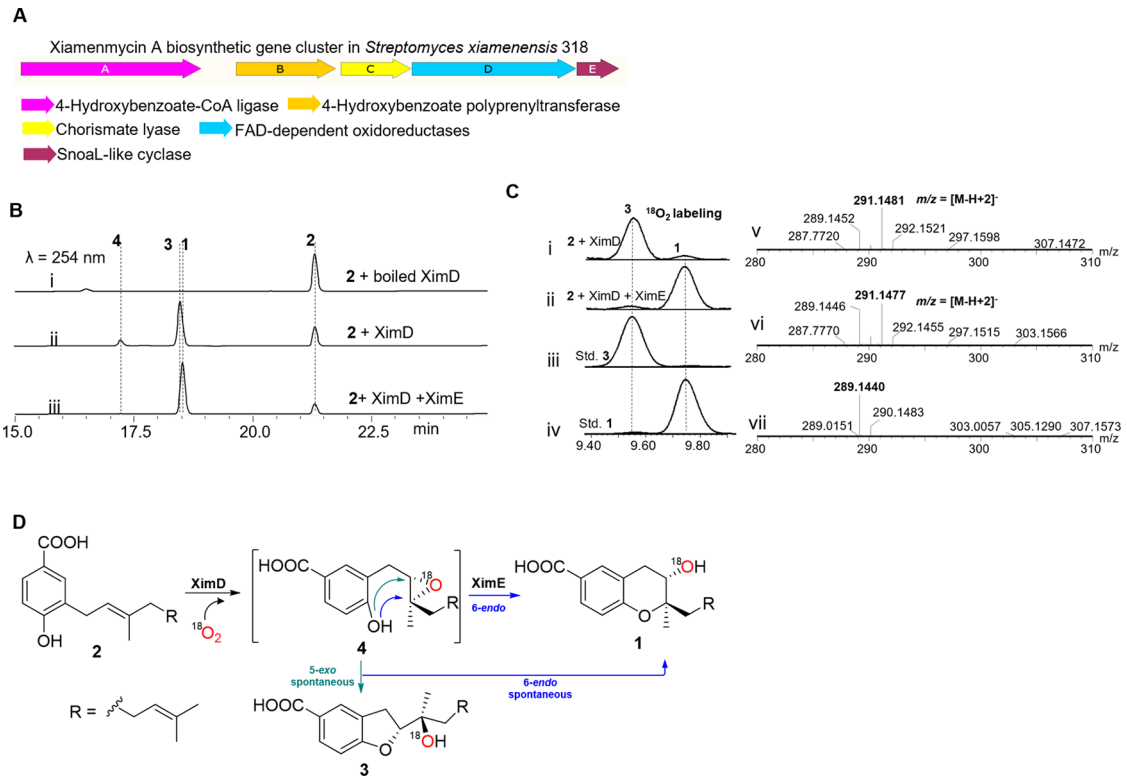

Figure 2. In vitro assay of XimD and XimE. (A) Xiamenmycin A biosynthetic gene cluster in *Streptomyces xiamenensis* 318. (B) Enzymatic assay of XimD and XimE: (i) compound **2** incubated with boiled XimD; (ii) **2** with XimD, FAD+, and NADH; (iii) **2** with XimD, FAD+, NADH, and XimE. Compounds **1** and **3** are overlapped by HPLC detection in (ii) and (iii). (C) UPLC-HRMS analysis of $^{18}O_2$ labeling experiment in the negative ionization mode: (i, ii) reaction product without and with XimE, respectively; (iii, iv) authentic **3** and **1**, respectively; (v–vii) mass spectra of compound **3** in (i), **1** in (ii), and authentic **3**, respectively. (D) Enzymatic conversions of **2** catalyzed by XimD in the presence and absence of XimE.

DOI: 10.1021/acscatal.9b01034
ACS Catal. 2019, 9, 5391–5399

to yield the precursor 3-geranyl-4-hydroxybenzoate (GBA, **2**). A gene deletion and complementation experiment had proved that the two downstream genes encode an FMO (*ximD*) and a SnoaL-like cyclase (*ximE*) that are essential for benzopyran formation during the biosynthesis of xiamenmycin.[19]

We previously showed that coexpression of *ximD* and *ximE* in an engineered *E. coli* strain (strain XM03-MVA[33]) that produces a high yield of the precursor GBA (**2**) results in the biosynthesis of **1**.[33] In this study, to clarify the role of XimD in this process, we overexpressed just *ximD* (without *ximE*) in strain XM03-MVA and compared the metabolic extracts with those from the parental strain using mass spectroscopy. We found that the extracts from the strain that solely overexpressed *ximD* contained an additional peak (**3**) with the precise expected mass of xiamenmycin B (**1**) ($[M - H]^-$, m/z 289.1446 for **1** and 289.1417 for **3**) (Figure S2). However, NMR spectroscopy clearly showed that this additional compound is actually benzodihydrofuran (**3**) (Table S1). Since XimD was annotated as a monooxygenase,[19] the identification of the unexpected compound **3** attracted us to further explore the enzymatic functions of XimD and XimE.

To investigate the roles of XimD and XimE, the recombinant proteins were overexpressed and purified to homogeneity as N-terminally His_6-tagged protein (Figure S3). XimD was previously predicted to be an FMO with a well-conserved FAD-binding motif (GXGXXG).[34] Consistent with this predication, we found that denaturation of XimD with methanol and subsequent HPLC analysis indicated that FAD is noncovalently bound to XimD at a molar ratio of FAD to protein of 0.93:1 (Figure S4). FMOs require NADH or NADPH as cofactor to perform the oxidative reactions.[35] Here, both NADH and NADPH can be used by XimD. However, XimD exhibits an obvious preference for NADH, because the consumption velocity of NADH is 6-fold that of NADPH (Figure S5). Thus, an in vitro assay of XimD was performed in the presence of **2**, NADH, and FAD, which yielded furan compound **3** and a trace amount of **4** (Figure 2B). It is consistent with the in vivo assay that overexpressing *ximD* in *E. coli* led to the formation of **3**. Compound **4** ($[M - H]^-$, m/z 289.1446) has an molecular weight identical with that of **1** and **3** and exhibits an ultraviolet−visible absorbance similar to that of **2** (Figure S6). We reasoned that this compound may be an epoxidized product of **2** which was catalyzed by XimD. This expectation was subsequently confirmed by a comparison of the retention time and mass spectrum of **4** with the product of a $VO(acac)_2$/TBHP system[24] catalyzed epoxidation using **2** as the starting material (Figure S7).

In the absence of XimE, the furan compound **3** is the dominant product, as shown in Figure 2C. When XimE was added, the benzopyran compound **1** was generated at an approximate ratio of **1** to **3** of 43:1 (the ratio of peak area), and the intermediate **4** was no longer present (Figure 2B,C). These results indicate that XimD catalyzes the monooxygenation of **2** to yield unstable **4**, which spontaneously converts to **3** in the absence of XimE and undergoes an anti-Baldwin cyclization to yield **1** in the presence of XimE (Figure 2D).

In the construction of a tetrahydrofuran or tetrahydropyran ring through an epoxide-opening reaction, the epoxide will either directly undergo a 6-endo-tet or a 5-exo-tet cyclization or be first hydrolyzed to form two hydroxy groups which then undergo a cyclization. The latter process occurs during the dioxabicyclooctane ring formation that is catalyzed by AurD,[5] where the oxygen of the C^5-hydroxy in the product is derived from H_2O.[5,36] To confirm the origin of the oxygen atom of the C^3-hydroxy in **1**, we conducted stable isotope labeling experiments of the in vitro assay. UPLC-MS analysis indicates that **1** and **3** were both labeled by the oxygen from $^{18}O_2$, instead of $H_2{}^{18}O$ (Figure 2C and Figure S8), no matter whether we used only XimD or both XimD and XimE.

Overall Structure of the Apo and Cocrystal of XimE. Sequence alignment and annotation showed that XimE belongs to the SnoaL-like cyclase family,[19,34] members of which include SnoaL[37] and AknH.[38] Both SnoaL and AknH catalyze intramolecular aldol condensation reactions to form an aromatic multicyclic ring system. Unlike SnoaL, however, XimE selectively catalyzes the C^2−O bond formation to generate a benzopyran skeleton. To understand the structural basis underlying the overwhelming selectivity of XimE in this catalysis, the crystal structure of apo XimE (PDB: 6ISK) was solved at a resolution of 1.77 Å by using selenomethionine (Se-Met) labeling and the single-wavelength anomalous diffraction method for phasing (Table S2). The subunit of XimE consists of one domain formed by three α-helices ($\alpha1$−$\alpha3$) and five β-sheets ($\beta1$−$\beta5$) (Figure 3A). The four antiparallel β-sheets

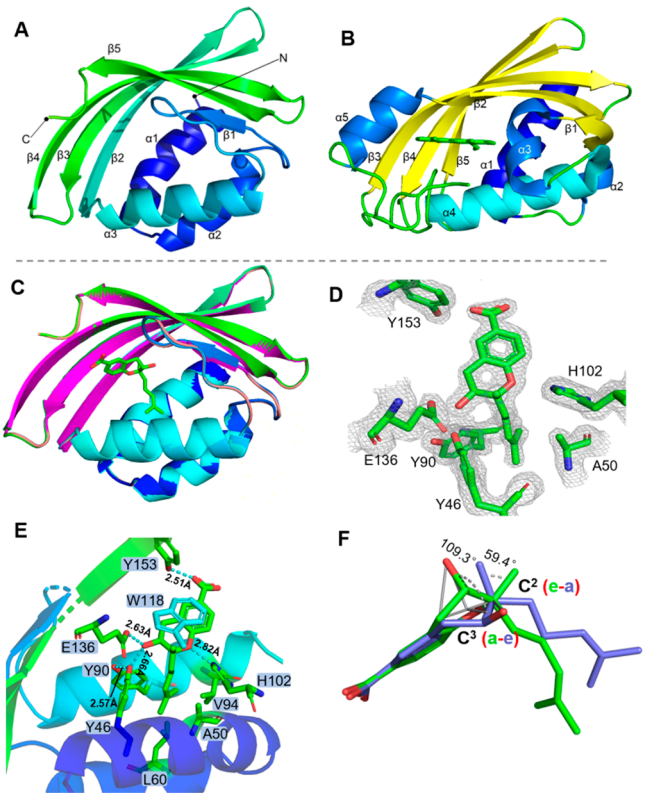

Figure 3. Overall fold of apo and cocrystal structures of XimE and SnoaL. (A) Apo structure of XimE (PDB code: 6ISK). (B) Cocrystal structure of SnoaL (PDB code: 1SJW). (C) Superimposition of apo and xiamenmycin B-bound structures (PDB code: 6ISL) of XimE. Xiamenmycin B (green stick) was found to fill in the cavity. (D) $2F_o - F_c$ electron density map for **1** and the surrounding residues, contoured at 2.0σ. The $F_o - F_c$ omit map of the ligand is presented in Figure S9. (E) Close-up view of the xiamenmycin B−XimE interactions. Dashed lines indicate hydrogen-bond interactions. Three β-sheets and one α-helix were removed to clarify the illustration. (F) Pair fit of free xiamenmycin B (green) and XimE-bound xiamenmycin B (indigo). The X-ray diffraction data of xiamenmycin B were deposited with the Cambridge Crystallographic Data Centre with the accession number CCDC 1871592.

DOI: 10.1021/acscatal.9b01034
ACS Catal. 2019, 9, 5391−5399

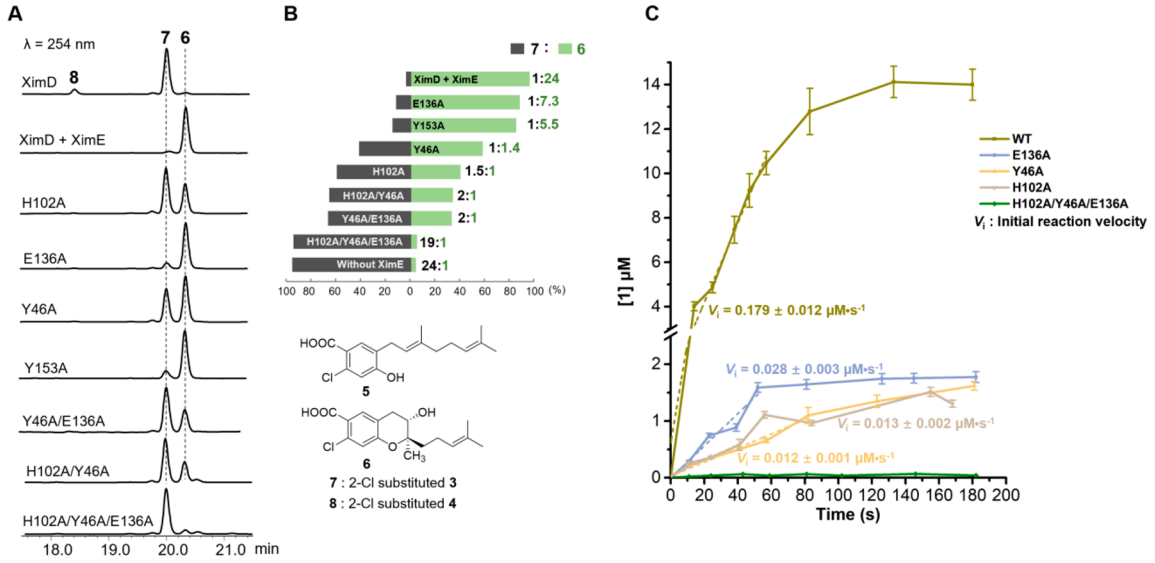

Figure 4. Enzymatic assay of XimE and various mutants. (A) HPLC profiles of an in vitro assay of XimE and various mutants by using **5** (2-Cl substituted **2**) as substrate. (B) Proportion of tetrahydrofuran (**7**) and tetrahydropyran (**6**) in the reaction products, calculated by the peak area. For each mutant, XimD was used to generate epoxide intermediate **8**. (C) Time-course analysis of the conversion of **4** to **1** in the presence of 40 nM XimE or mutants. The isomers of **4** were used as substrate. We performed the in vitro experiment on ice (0 °C) to slow down the reaction rate. The concentration of pyran product **1** and initial reaction time was fitted to a linear function (dashed lines) by Origin (OriginLab, Northampton, MA) to obtain the initial reaction rate, V_i. The V_i value consists of enzymatic transformation $V_{E(6\text{-m-r})}$ (6-m-r = 6-membered ring) and nonenzymatic conversion rate $V_{non(6\text{-m-r})}$: i.e., $V_i = V_{E(6\text{-m-r})} + V_{non(6\text{-m-r})}$. However, $V_{non(6\text{-m-r})}$ is negligible under the current reaction conditions: phosphate buffer with a pH value of 9.58. V_i thus can be the close approximation of $V_{E(6\text{-m-r})}$.

($\beta2-\beta5$) are continuous in the primary sequence and are considerably curved in the structure, encircling to form part of a barrel-like architecture. The additional β-strand ($\beta1$) parallels with $\beta5$, and its C-terminus and N-terminus form two short loops. These two loop motifs and the three α-helices close off the barrel-like structure and form a deep hydrophobic cavity.

A query of the PDB database using the DALI program[39] revealed several different enzymes that are structurally similar to XimE (Table S3). Among the 55 most closely related targets, 16 of them are SnoaL-like polyketide cyclases and 9 of them are ketosteroid isomerases. None of these enzymes, however, shows high primary sequence identity to XimE and so can be grouped into a similar "SnoaL-like fold" family on the basis of their structural similarity.[40] A comparison of XimE with the well-characterized polyketide cyclases SnoaL and AknH, indicates that the folding manner of XimE is nearly identical with those of SnoaL and AknH[37,38,41] (Figure 3B), although XimE exists as a homodimer and SnoaL exists as a dimer of dimers.[37] Thus, together with the NCBI blastp prediction,[19] this structural comparison unequivocally indicates that XimE is a member of the SnoaL-like cyclases.

However, the observed overall structure of apo XimE does not suggest an obvious candidate for the active sites of substrate binding and catalysis. We thus determined the 1.77 Å resolution structure of XimE bound to xiamenmycin B (Figure 3C and Table S2; PDB code: 6ISL). Globally, the ligand-bound and apo structures are nearly identical, with an rms deviation of 0.141 Å over 227 atoms (including ligands). In the cocrystal structure of XimE, xiamenmycin B (**1**) is buried in the pocket of the barrel-like region which was filled by the buffer molecules malonic acid (chain A) and ethylene glycol (chain B) in the apo XimE (Figure 3C,D and Figure S9). The prenyl moiety of **1** is fully extended inside the pocket and contacts the hydrophobic residues, such as Ala50, Leu60, and Val94. In addition, the carboxyl group points to the mouth of the pocket and is anchored by a hydrogen-bond interaction with Tyr153 (Figure 3E). In particular, the oxygen atom O1 of the pyran ring is found to form a hydrogen bond with the imidazole group of His102. Further, the carboxyl group of Glu136 is almost rotated by 100° to allow bifurcated hydrogen-bonding interactions with the hydroxyl O4. Furthermore, the $\pi-\pi$ stacking interaction between the phenyl ring of xiamenmycin B and Trp118 is observed. These specific interactions with the protein change the pyran conformation of xiamenmycin B: i.e., the equatorial orientation of the C^2-CH_3 group in isolated xiamenmycin B turns into an axial orientation and the axial C^3-OH is flipped to an equatorial orientation (Figure 3F). Interestingly, a hydrogen-bonding network with Tyr90 is found to enhance the polarity of Tyr46 (Figure S10).[42]

Cooperative Roles of Active Sites in XimE. Inspection of the apo and cocrystal structures led to the identification of Tyr46, His102, Glu136, and Y153 as possible key residues for the pyran ring formation. To test this, we examined the activity of single-point mutants of XimE in which each of these residues were mutated to alanine, using a 2-Cl-substituted GBA[33] molecule (**5**) as a surrogate in vitro, since its pyran-containing (**6**) and furan-containing (**7**) products can be clearly separated by HPLC. In comparison to wild type XimE (where the **7**:**6** ratio is 1:24), both H102A and Y46A mutants yielded a greater accumulation of **7**, exhibiting **7**:**6** ratios of 1.5:1 and 1:1.4, respectively (Figure 4A,B). This accumulation is likely due to a subnormal activity of the mutants, leading to a nonenzymatic cyclization of the epoxide (**8**). Overall, we found that the catalytic selectivity of all of the single-point mutants was decreased (Figure 4A,B). However, interestingly, the 6-endo-tet ring closure activity is not completely absent in any of them, which suggests that the 6-endo cyclization involves multiple residues. We hence constructed double (Y46A/H102A and Y46A/E136A) and triple (Y46A/H102A/E136A)

DOI: 10.1021/acscatal.9b01034
ACS Catal. 2019, 9, 5391−5399

mutants to further localize the essential sites. We found that Y46A/H102A was even further attenuated in pyran formation (2:1), whereas Y46A/H102A/E136A exhibited almost no 6-endo catalytic ability (19:1) (Figure 4A,B).

We tried to determine the steady-state enzyme kinetics value of each mutant in order to compare their activities. However, the instability of epoxide **4** impeded the purification and characterization of wild type XimE and its mutants. The rapid nonenzymatic conversion of **4** was observed in varied solutions (Figure S11). In phosphate buffer (5% ACN, pH 8.0, 22 °C), the first-order rate constant k_{non} was determined to be 1.3×10^{-3} s^{-1}, with a half-time of 8.9 min. Alternatively, we performed the time-course analysis of the conversion from **4** to **1** at low temperature (0 °C) to compare the relative activity of each variant (Figure 4C and Figure S12). The initial reaction rate of wild type XimE was determined as 0.179 ± 0.012 μM s^{-1}. The single mutants E136A, Y46A, and H102A exhibited a dramatic decrease in velocities, with initial rates of 0.028 ± 0.003, 0.012 ± 0.001, and 0.013 ± 0.002 μM s^{-1}, respectively. Additionally, the circular dichroism (CD) spectra of mutants revealed the fluctuation of absorbance between 190 and 200 nm (Figure S13), suggesting that these residues may play an important role in stabilizing the secondary structure of XimE. Collectively, the mutational experiments suggest that the residues E136A, Y46A, and H102A are functionally important to catalysis, substrate binding, and structural stabilization.

Regioselectivity of XimE. We further used QM/MM calculation to study the reaction energy potential surface of the 6-endo cyclization (Figure 5A,B). As a result, a water molecule was found be involved in the hydrogen-bond network of Tyr46−Tyr90−Glu136 that plays a general-acid role in the transition state. This indicates that the protonation process is promoted by both Tyr46 and Glu136, rationalizing the complicated effect observed in the mutagenesis experiment. Protonation of the epoxide results in the electron deficiency of carbon atoms of C2 and C3, especially C2, which can be stabilized by other two substituents, which are thereby vulnerable to nucleophilic group. Notably, due to the hydrogen bond network formed between the epoxide oxygen atom and hydroxy groups of Glu136 and Tyr46 which is mediated by a water molecule, the epoxide ring is stretched to be a nonisosceles configuration. The 1.87 Å length of C^2−O is more unstable than C^3−O, which is the canonical 1.41 Å in length, the same as the epoxide motif present in the cocrystal structure of Lsd19 with its substrate analogue[8] (Figure 5C). In addition, the distance (2.09 Å) between *p*-OH and carbon atom C2 of the substrate is closer than that (2.63 Å) of between *p*-OH and C3 (Figure 5B). Moreover, imidazole of His102 points the *p*-OH at about 2.50 Å and is proposed to deprotonate the phenol hydroxyl group to form a nucleophilic phenolate anion that is also stabilized by imidazole of His102, a similar function of the amino group of His107 in SnoaL.[37] Taken together, the activated epoxide thus accepts regioselectively nucleophilic attack at C2 by phenolate anion, giving rise to the formation of a pyran ring (Figure 6).

The QM/MM calculation and the crystal structures indicated that XimE-catalyzed pyran ring formation is mainly realized by protonation and stabilization of epoxide by the catalytic acidic residues Tyr46 and Glu136 and basic residue His102. Particularly, the acidic condition is essential for the pyran ring formation. To verify this hypothesis, the nonenzymatic transformation was carried out in aqueous phases with different pH values. With a decrease in pH, a shift was

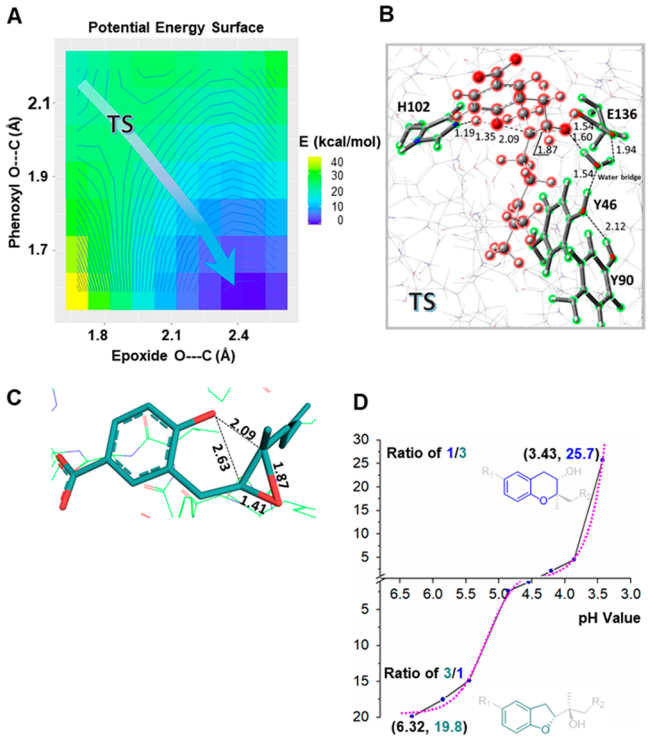

Figure 5. Computational studies of XimE-catalyzed 6-endo cyclization. (A) Potential energy surface of C−O bonds in the transition state. (B) Transition state of epoxide opening ring closure in a 6-endo-tet manner. The black dashed lines indicate H bonds and water bridge. (C) Configuration of **4** in the catalytic pocket of XimE. (D) Nonenzymatic conversion of **4** to **1** and **3** in aqueous phases with different pH values. The ratio of **1** to **3** (and **3** to **1**) and pH values were fitted to the BiDoseResp function by Origin (OriginLab, Northampton, MA) to obtain the sigmoidal curve, with R^2 values of 0.998.

found from the furan-favored compound **3** under basic conditions to the pyran-favored compound **1** under acidic conditions (Figure 5D and Figure S14). When the pH is 6.32, benzofuran is predominant, in which the ratio of pyran (**1** + **1′**) to furan (**3** + **3′**) is 1:19.8. Under acidic conditions, e.g., at pH 3.43, the benzopyran form is the major product with a ratio of pyran to furan of 25:1 (Figure 5D). The pH-dependent transformation agrees with a hypothetical synergistic mechanism in which the protonated pathway prefers a pyran form, while the deprotonated conditions prefer furan in the calculations (Figure S15). We noted that **1′** is not increased in the in vitro reactions by using stereoisomers **4** + **4′** as substrate (Figure S12), which indicates that XimE is unable to transform **4′** into **1′**. We speculate that when **4′** was accommodated by XimE, the opposite configuration of the epoxide either is energetically unstable in the cavity or cannot be activated by the catalytic residues to accept nucleophilic attack in a manner of 6-endo-tet cyclization (Figure S16).

Pyran ring formation reactions are also found in the biosynthesis of bacterial and fungal polyketides:[1,3−5,8] e.g., Lsd19-catalyzed lasalocid A formation, AurD-catalyzed aurovertin E formation, and biosynthesis of salinomycin catalyzed by SalBIII. However, very limited identity (less than 16% with any of them) (Table S4) in the primary sequence between XimE and these enzymes leads to a remarkable divergence in phylogenetic tree and significant difference in the 3D structure (RMSD = 4.964 Å with Lsd19B) and active-site organization

DOI: 10.1021/acscatal.9b01034
ACS Catal. 2019, 9, 5391−5399

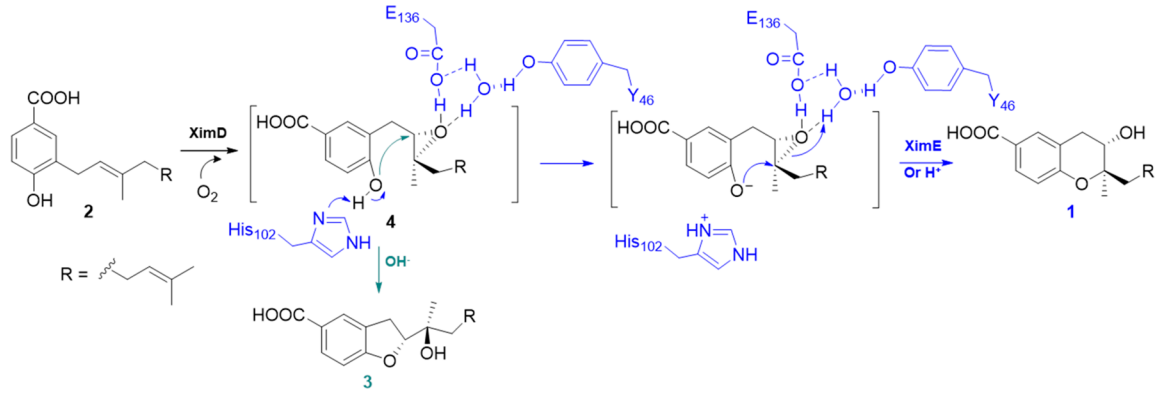

Figure 6. Proposed mechanism of XimE-catalyzed pyran ring formation and spontaneous transformation from **4** to **1** and **3**.

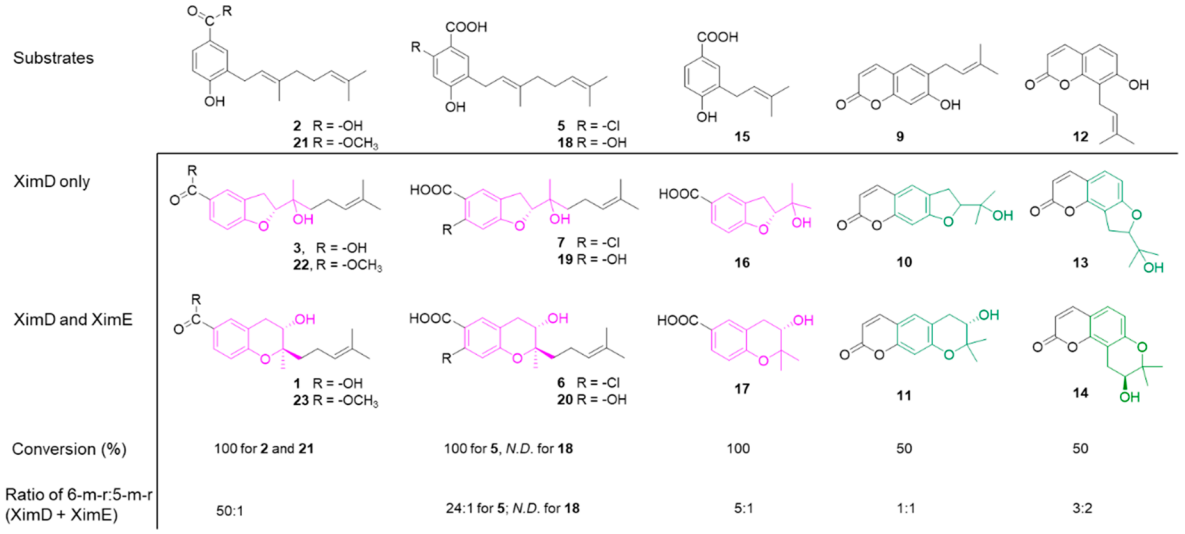

Figure 7. Substrate scope of XimE and XimD. Successfully obtained products are benzodihydrofuran (**3**, **7**, **16**, **19**, **22**), benzodihydropyran (**1**, **6**, **17**, **20**, **23**), furanocoumarin (**10**, **13**), and pyranocoumarin (**11**, **14**) scaffolds, which are highlighted by different colors. The conversion rate represents the percentage of transformed substrate in vitro under the same catalytic conditions and was estimated by HPLC analysis. The ratio 6-m-r:5-m-r represents the relative amount of pyran product to furan product, which was estimated by peak areas in HPLC analysis. For HPLC and HRMS data see Figures S20−S23. Several unsuccessfully transformed substrates are summarized in Figure S24.

(Figures S17 and S18). This indicates that XimE had optimally tuned to be a SnoaL-like cyclase that specifically catalyzes benzopyran skeleton formation.

Structure-Based Substrate Scope. The critical role of XimE is to spatially orient the epoxide for exclusively nucleophilic attack at C2 and allow reasonable variation at the substrate. We proposed that other substitution on the benzene ring will not affect 6-endo cyclization, as we have proved this by using 2-Cl-substituted GBA as a surrogate. 2-Chloro substitution could also be replaced by other groups, such as 2-hydroxyl as shown in Figure 7. Furthermore, because the aromatic ring is oriented to the outside of the catalytic pocket (Figure S19), other benzoheterocycle skeletons might also be tolerant to XimE. 7-Demethylsuberosin (**9**), the putative precursor of linear pyranocoumarin decursinol,[43] was used as a substrate to verify our assumption. The analysis of reaction products revealed the formation of marmesin (**10**); $[M - H]^+$, m/z 247.0970) without XimE, and decursinol (**11**; $[M - H]^+$, m/z 247.0967) appeared in the presence of XimE. This result was confirmed by a comparison of retention times and accurate masses with the authentic samples by UPLC-QTOF-MS (Figure S20). By using osthenol (**12**) as substrate, the combination of XimD and XimE could also produce the angular furanocoumarin columbianetin (**13**; $[M - H]^+$, m/z 247.0969) and pyranocoumarin lomatin (**14**; $[M - H]^+$, m/z 247.0971) (Figure S21). We successfully obtained 14 products with 6 different benzoheterocycle scaffolds by using XimD and XimE as catalysts, as summarized in Figure 7.

The enzymes responsible for the conversion of 7-demethylsuberosin to decursinol in the plant *Angelica gigas*, and the biosynthesis from osthenol to lomatin or columbianetin in *Lomatium nutalli* have been longstanding mysteries.[43−47] Nevertheless, the widespread use of coumarins in traditional and modern medicine[29,48−50] has triggered extensive effort toward their biosynthesis in microbes.[51−53] Due to the unavailability of enzyme tools (Figure S25), the most common ways of getting coumarins are through plant cell extraction or chemical synthesis. Only simple coumarins have been obtained in the manner of microbial synthesis until now: i.e., the biosynthesis of umbelliferone, scopoletin, and 4-hydroxycoumarin[52] in engineered *E. coli*. Thus, by incorporation with the recently identified umbelliferone 6-dimethylallyltransferase and 8-dimethylallyltransferase[43] that respectively catalyze the formation of **9** and **12**, the well-characterized XimD and XimE will be promising downstream enzymes for

DOI: 10.1021/acscatal.9b01034
ACS Catal. 2019, 9, 5391−5399

furanocoumarin and pyranocoumarin biosynthesis in *E. coli* or yeast.

Using microbe-derived enzymes as alternatives to fill in the missing gaps in phytochemical biosynthetic pathways is an attractive approach.[54] This strategy leverages the promiscuity of catalytic enzymes, especially those involved in secondary metabolite biosynthesis, and thus yields a pool of potential candidates for combinatory biosynthesis. Outstanding examples include the biosynthesis of (−)-menthol using Δ5−3-ketosteroid isomerase from *Pseudomonas putida*[55] and the reconstruction of dopamine in *E. coli* using the *Streptomyces castaneoglobisporus* tyrosinase and *Pseudomonas putida* L-DOPA decarboxylase.[56] These cases have showcased that, by fully releasing the catalytic potential of enzymes, the aforementioned strategy will enable the efficient and renewable biosynthesis of important plant natural products in a microbial system from simple carbon sources.

CONCLUSIONS

In this study, we determined the biosynthetic mechanism by which the pyran ring of xiamenmycin is formed. The SnoaL-like cyclase XimE catalyzes a pyran-forming reaction by mediating the intramolecular attack of a phenolate anion onto the epoxide moiety of the epoxidized form of 3-geranyl-4-hydroxybenzoic acid. We demonstrated the critical importance of the catalytic dyad Y46−E136, acting as a general acid, of this enzyme in establishing the proper spatial organization of the epoxide and controlling the substrate preference of the nucleophilic attack. The unique architecture of the catalytic pocket and the precise chemical reaction that it catalyzes was found to permit a high flexibility on potential substrates for this enzyme. Indeed, the catalytic versatility of XimE and XimD functioning together strongly suggests that these novel enzymes may become highly effective tools for the chemoenzymatic synthesis of many bioactive benzoheterocycle scaffolds, including benzofurans and benzopyrans, as well as plant-derived linear and angular furano- and pyranocoumarins. The rational expansion of substrates we demonstrated here also provides a promising strategy for future microbial synthesis of high-value phytochemicals.

ASSOCIATED CONTENT

Supporting Information

The Supporting Information is available free of charge on the ACS Publications website at DOI: 10.1021/acscatal.9b01034.

^{1}H, ^{13}C, and 2D NMR spectra and HRESIMS spectra of **3**, **6**, and **20**, CD data for mutants, data collection and refinement statistics for X-ray diffraction experiments, HPLC analysis of the transformation of **4**, and experimental details (PDF)

AUTHOR INFORMATION

Corresponding Authors

*E-mail for J.-T.Z.: jtzheng@sjtu.edu.cn.
*E-mail for Y.-L.Z.: yileizhao@sjtu.edu.cn.
*E-mail for M.-J.X.: minjuanxu@sjtu.edu.cn.

ORCID

Jun Xu: 0000-0001-6221-4627
Shuangjun Lin: 0000-0001-9406-9233
Jian-Ting Zheng: 0000-0003-1250-3556
Yi-Lei Zhao: 0000-0003-4687-7847
Min-Juan Xu: 0000-0003-1768-208X

Author Contributions

M.-J.X., Y.-L.Z., J.X., and B.-B.H. designed the study. B.-B.H., J.-T.Z., and T.Z. performed the crystal structural determination. B.-B.H. performed the in vitro and in vivo assay. B.-B.H., X.-L.B., J.-Y.W., and T.Z. extracted and purified the compounds. M.-J.X. elucidated the structures. Y.-L.Z. performed the computational experiments. All authors analyzed and discussed the results. B.-B.H., S.L., Y.-L.Z., J.X. and M.-J.X. prepared the manuscript with input from all of the authors. All authors have given approval to the final version of the manuscript.

Funding

This work was supported by the National Natural Science Foundation of China 81473105. Y.L. Zhao thanks the National Natural Science Foundation of China (31770070 and 21377085).

Notes

The authors declare no competing financial interest.

ACKNOWLEDGMENTS

We thank B. N. Dai and J. L. Wu for the NMR experiments, R. B. Wang for the CD and optical rotation measurements, L. Feng and J. Gui for UPLC-MS, and X. L. Bao and L. L. Li for X-ray crystallographic analysis at the Instrumental Analysis Center of Shanghai Jiao Tong University. The protein diffraction data were collected at Shanghai Synchrotron Radiation Facility (SSRF) beamlines BL17U1, BL18U, and BL19U. We thank Dr. X. X. Guo and Z. Y. Hu for the chemical synthesis of epoxide. We are grateful to Prof. S.-M. Li, Prof. Y. Tang, and Prof. P. Xie for fruitful discussions and Prof. D. Czajkowsky for great help during the preparation of this manuscript.

REFERENCES

(1) Luhavaya, H.; Dias, M. V. B.; Williams, S. R.; Hong, H.; de Oliveira, L. G.; Leadlay, P. F. Enzymology of Pyran Ringa Formation in Salinomycin Biosynthesis. *Angew. Chem., Int. Ed.* **2015**, *54*, 13622−13625.

(2) Berkhan, G.; Hahn, F. A. Dehydratase Domain in Ambruticin Biosynthesis Displays Additional Activity as a Pyran-Forming Cyclase. *Angew. Chem., Int. Ed.* **2014**, *53*, 14240−14244.

(3) Minami, A.; Ose, T.; Sato, K.; Oikawa, A.; Kuroki, K.; Maenaka, K.; Oguri, H.; Oikawa, H. Allosteric Regulation of Epoxide Opening Cascades by a Pair of Epoxide Hydrolases in Monensin Biosynthesis. *ACS Chem. Biol.* **2014**, *9*, 562−569.

(4) Minami, A.; Shimaya, M.; Suzuki, G.; Migita, A.; Shinde, S. S.; Sato, K.; Watanabe, K.; Tamura, T.; Oguri, H.; Oikawa, H. Sequential Enzymatic Epoxidation Involved in Polyether Lasalocid Biosynthesis. *J. Am. Chem. Soc.* **2012**, *134*, 7246−7249.

(5) Mao, X. M.; Zhan, Z. J.; Grayson, M. N.; Tang, M. C.; Xu, W.; Li, Y. Q.; Yin, W. B.; Lin, H. C.; Chooi, Y. H.; Houk, K. N.; Tang, Y. Efficient Biosynthesis of Fungal Polyketides Containing the Dioxabicyclo-Octane Ring System. *J. Am. Chem. Soc.* **2015**, *137*, 11904−11907.

(6) Shoyama, Y.; Tamada, T.; Kurihara, K.; Takeuchi, A.; Taura, F.; Arai, S.; Blaber, M.; Shoyama, Y.; Morimoto, S.; Kuroki, R. Structure and Function of 1-Tetrahydrocannabinolic Acid (THCA) Synthase, the Enzyme Controlling the Psychoactivity of *Cannabis sativa*. *J. Mol. Biol.* **2012**, *423*, 96−105.

(7) Iijima, M.; Munakata, R.; Takahashi, H.; Kenmoku, H.; Nakagawa, R.; Kodama, T.; Asakawa, Y.; Abe, I.; Yazaki, K.; Kurosaki, F.; Taura, F. Identification and Characterization of Daurichromenic Acid Synthase Active in Anti-Hiv Biosynthesis. *Plant Physiol.* **2017**, *174*, 2213−2230.

DOI: 10.1021/acscatal.9b01034
ACS Catal. 2019, 9, 5391−5399

(8) Hotta, K.; Chen, X.; Paton, R. S.; Minami, A.; Li, H.; Swaminathan, K.; Mathews, I. I.; Watanabe, K.; Oikawa, H.; Houk, K. N.; Kim, C. Y. Enzymatic Catalysis of Anti-Baldwin Ring Closure in Polyether Biosynthesis. *Nature* **2012**, *483*, 355−358.
(9) Tang, M.-C.; Zou, Y.; Watanabe, K.; Walsh, C. T.; Tang, Y. Oxidative Cyclization in Natural Product Biosynthesis. *Chem. Rev.* **2017**, *117*, 5226−5333.
(10) Helfrich, E. J. N.; Piel, J. Biosynthesis of Polyketides by *trans*-AT Polyketide Synthases. *Nat. Prod. Rep.* **2016**, *33*, 231−316.
(11) Wagner, D. T.; Zhang, Z.; Meoded, R. A.; Cepeda, A. J.; Piel, J.; Keatinge-Clay, A. T. Structural and Functional Studies of a Pyran Synthase Domain from a *trans*-Acyltransferase Assembly Line. *ACS Chem. Biol.* **2018**, *13*, 975−983.
(12) Marcos, R.; Rodriguez-Escrich, C.; Herrerias, C. I.; Pericas, M. A. Metal-Mediated Cyclization of Aryl and Benzyl Glycidyl Ethers: A Complete Scenario. *J. Am. Chem. Soc.* **2008**, *130*, 16838−16839.
(13) Shi, Z.; He, C. An Au-Catalyzed Cyclialkylation of Electron-Rich Arenes with Epoxides to Prepare 3-Chromanols. *J. Am. Chem. Soc.* **2004**, *126*, 5964−5965.
(14) Birringer, M.; Siems, K.; Maxones, A.; Frank, J.; Lorkowski, S. Natural 6-Hydroxy-Chromanols and -Chromenols: Structural Diversity, Biosynthetic Pathways and Health Implications. *RSC Adv.* **2018**, *8*, 4803−4841.
(15) Tamemoto, K.; Takaishi, Y.; Chen, B.; Kawazoe, K.; Shibata, H.; Higuti, T.; Honda, G.; Ito, M.; Takeda, Y.; Kodzhimatov, O. K.; Ashurmetov, O. Sesquiterpenoids from the Fruits of *Ferula kuhistanica* and Antibacterial Activity of the Constituents of *F. Kuhistanica*. *Phytochemistry* **2001**, *58*, 763−767.
(16) Chen, B.; Kawazoe, K.; Takaishi, Y.; Honda, G.; Itoh, M.; Takeda, Y.; Kodzhimatov, O. K.; Ashurmetov, O. Prenylated Benzoic Acid Derivatives from *Ferula Kuhistanica*. *J. Nat. Prod.* **2000**, *63*, 362−365.
(17) Yim, D.; Singh, R. P.; Agarwal, C.; Lee, S.; Chi, H.; Agarwal, R. A Novel Anticancer Agent, Decursin, Induces G_1 Arrest and Apoptosis in Human Prostate Carcinoma Cells. *Cancer Res.* **2005**, *65*, 1035−1044.
(18) Liu, X. J.; Xu, M. J.; Fan, S. T.; Wu, Z.; Li, J.; Yang, X. M.; Wang, Y. H.; Xu, J.; Zhang, Z. G. Xiamenmycin Attenuates Hypertrophic Scars by Suppressing Local Inflammation and the Effects of Mechanical Stress. *J. Invest. Dermatol.* **2013**, *133*, 1351−1360.
(19) Yang, Y.; Fu, L.; Zhang, J.; Hu, L.; Xu, M.; Xu, J. Characterization of the Xiamenmycin Biosynthesis Gene Cluster in *Streptomyces Xiamenensis* 318. *PLoS One* **2014**, *9*, No. e99537.
(20) Jacolot, M.; Jean, M.; Tumma, N.; Bondon, A.; Chandrasekhar, S.; van de Weghe, P. Synthesis of Stachybotrin C and All of Its Stereoisomers: Structure Revision. *J. Org. Chem.* **2013**, *78*, 7169−7175.
(21) Kawamura, K.; Ohta, T.; Otani, G. A New Method for the Synthesis of 3-Chromanol Derivatives by Sodium Iodide-Catalyzed Cyclization of Epoxide. *Chem. Pharm. Bull.* **1990**, *38*, 2088−2091.
(22) Lee, J. H.; Bang, H. B.; Han, S. Y.; Jun, J. G. An Efficient Synthesis of (+)-Decursinol from Umbelliferone. *Tetrahedron Lett.* **2007**, *48*, 2889−2892.
(23) Page, P. C.; Appleby, L. F.; Day, D.; Chan, Y.; Buckley, B. R.; Allin, S. M.; McKenzie, M. J. Highly Enantioselective Total Synthesis of (−)-(3′*S*)-Lomatin and (+)-(3′*S*,4′*R*)-*trans*-Khellactone. *Org. Lett.* **2009**, *11*, 1991−1993.
(24) Lattanzi, A.; Scettri, A. Vo(Acac)$_2$/TBHP Catalyzed Epoxidation of 2-(2-Alkenyl)Phenols. Highly Regio- and Diastereoselective Oxidative Cyclization to 2,3-Dihydrobenzofuranols and 3-Chromanols. *Synlett.* **2002**, *2002*, 0942−0946.
(25) Yao, Y.-Y.; Liu, X.-Y.; Li, X.-Y.; Yang, H.-G.; Li, L.; Jiao, X.-Z.; Xie, P. Total Synthesis of Xiamenmycin C and All of Its Stereoisomers: Stereochemical Revision. *J. Asian Nat. Prod. Res.* **2016**, *18*, 976−987.
(26) Kim, K. Y.; Lee, S.; Cha, C. J. Biotransformation of Plant Secondary Metabolite Decursin by *Mycobacterium* Sp. Pyr1001. *J. Agric. Food Chem.* **2010**, *58*, 2931−2934.
(27) Rhee, H. S.; Cho, H. Y.; Son, S. Y.; Yoon, S. Y. H.; Park, J. M. Enhanced Accumulation of Decursin and Decursinol Angelate in Root Cultures and Intact Roots of *Angelica gigas* Nakai Following Elicitation. *Plant Cell, Tissue Organ Cult.* **2010**, *101*, 295−302.
(28) Park, N. I.; Park, J. H.; Park, S. U. Overexpression of Cinnamate 4-Hydroxylase Gene Enhances Biosynthesis of Decursinol Angelate in *Angelica gigas* Hairy Roots. *Mol. Biotechnol.* **2012**, *50*, 114−120.
(29) Duarte, J.; Vallejo, I.; PerezVizcaino, F.; Jimenez, R.; Zarzuelo, A.; Tamargo, J. Effects of Visnadine on Rat Isolated Vascular Smooth Muscles. *Planta Med.* **1997**, *63*, 233−236.
(30) Matsumoto, N.; Suzuki, E.; Ishikawa, M.; Shirafuji, T.; Hasumi, K. Soluble Epoxide Hydrolase as an Anti-Inflammatory Target of the Thrombolytic Stroke Drug SMTP-7. *J. Biol. Chem.* **2014**, *289*, 35826−35838.
(31) Koide, H.; Narasaki, R.; Hasegawa, K.; Nishimura, N.; Hasumi, K. A New Series of the SMTP Plasminogen Modulator with a Phenylglycine-Based Side Chain. *J. Antibiot.* **2012**, *65*, 91−93.
(32) Nozawa, Y.; Yamamoto, K.; Ito, M.; Sakai, N.; Mizoue, K.; Mizobe, F.; Hanada, K. Stachybotrin C and Parvisporin, Novel Neuritogenic Compounds. I. Taxonomy, Isolation, Physico-Chemical and Biological Properties. *J. Antibiot.* **1997**, *50*, 635−640.
(33) He, B. B.; Bu, X. L.; Zhou, T.; Li, S. M.; Xu, M. J.; Xu, J. Combinatory Biosynthesis of Prenylated 4-Hydroxybenzoate Derivatives by Overexpression of the Substrate-Promiscuous Prenyltransferase XimB in Engineered *E. coli*. *ACS Synth. Biol.* **2018**, *7*, 2094−2104.
(34) Marchler-Bauer, A.; Bo, Y.; Han, L.; He, J.; Lanczycki, C. J.; Lu, S.; Chitsaz, F.; Derbyshire, M. K.; Geer, R. C.; Gonzales, N. R.; Gwadz, M.; Hurwitz, D. I.; Lu, F.; Marchler, G. H.; Song, J. S.; Thanki, N.; Wang, Z.; Yamashita, R. A.; Zhang, D.; Zheng, C.; Geer, L. Y.; Bryant, S. H. Cdd/Sparcle: Functional Classification of Proteins via Subfamily Domain Architectures. *Nucleic Acids Res.* **2017**, *45*, D200−D203.
(35) van Berkel, W. J. H.; Kamerbeek, N. M.; Fraaije, M. W. Flavoprotein Monooxygenases, a Diverse Class of Oxidative Biocatalysts. *J. Biotechnol.* **2006**, *124*, 670−689.
(36) Steyn, P. S.; Vleggaar, R. Mechanistic Studies on the Biosynthesis of the Aurovertins Using ^{18}O-Labelled Precursors. *J. Chem. Soc., Chem. Commun.* **1985**, *0*, 1796−1798.
(37) Sultana, A.; Kallio, P.; Jansson, A.; Wang, J. S.; Niemi, J.; Mantsala, P.; Schneider, G. Structure of the Polyketide Cyclase Snoal Reveals a Novel Mechanism for Enzymatic Aldol Condensation. *EMBO J.* **2004**, *23*, 1911−1921.
(38) Kallio, P.; Sultana, A.; Niemi, J.; Mantsala, P.; Schneider, G. Crystal Structure of the Polyketide Cyclase Aknh with Bound Substrate and Product Analogue: Implications for Catalytic Mechanism and Product Stereoselectivity. *J. Mol. Biol.* **2006**, *357*, 210−220.
(39) Holm, L.; Rosenstrom, P. Dali Server: Conservation Mapping in 3D. *Nucleic Acids Res.* **2010**, *38*, W545−W549.
(40) Fox, N. K.; Brenner, S. E.; Chandonia, J. M. Scope: Structural Classification of Proteins-Extended, Integrating Scop and Astral Data and Classification of New Structures. *Nucleic Acids Res.* **2014**, *42*, D304−D309.
(41) Beinker, P.; Lohkamp, B.; Peltonen, T.; Niemi, J.; Mantsala, P.; Schneider, G. Crystal Structures of SnoaL2 and AclR: Two Putative Hydroxylases in the Biosynthesis of Aromatic Polyketide Antibiotics. *J. Mol. Biol.* **2006**, *359*, 728−740.
(42) Wu, Y.; Boxer, S. G. A Critical Test of the Electrostatic Contribution to Catalysis with Noncanonical Amino Acids in Ketosteroid Isomerase. *J. Am. Chem. Soc.* **2016**, *138*, 11890−11895.
(43) Munakata, R.; Olry, A.; Karamat, F.; Courdavault, V.; Sugiyama, A.; Date, Y.; Krieger, C.; Silie, P.; Foureau, E.; Papon, N.; Grosjean, J.; Yazaki, K.; Bourgaud, F.; Hehn, A. Molecular Evolution of Parsnip (*Pastinaca sativa*) Membrane-Bound Prenyltransferases for Linear and/or Angular Furanocoumarin Biosynthesis. *New Phytol.* **2016**, *211*, 332−344.

DOI: 10.1021/acscatal.9b01034
ACS Catal. 2019, 9, 5391−5399

(44) Park, J. H.; Park, N. I.; Xu, H.; Park, S. U. Cloning and Characterization of Phenylalanine Ammonia-Lyase and Cinnamate 4-Hydroxylase and Pyranocoumarin Biosynthesis in *Angelica gigas*. *J. Nat. Prod.* **2010**, *73*, 1394−1397.
(45) Gomez-Robledo, H. B.; Cruz-Sosa, F.; Bernabe-Antonio, A.; Guerrero-Analco, A.; Olivares-Romero, J. L.; Alonso-Sanchez, A.; Villafan, E.; Ibarra-Laclette, E. Identification of Candidate Genes Related to Calanolide Biosynthesis by Transcriptome Sequencing of *Calophyllum brasiliense* (Calophyllaceae). *BMC Plant Biol.* **2016**, *16*, 177.
(46) Larbat, R.; Hehn, A.; Hans, J.; Schneider, S.; Jugde, H.; Schneider, B.; Matern, U.; Bourgaud, F. Isolation and Functional Characterization of *CYP71AJ4* Encoding for the First P450 Monooxygenase of Angular Furanocoumarin Biosynthesis. *J. Biol. Chem.* **2009**, *284*, 4776−4785.
(47) Larbat, R.; Kellner, S.; Specker, S.; Hehn, A.; Gontier, E.; Hans, J.; Bourgaud, F.; Matern, U. Molecular Cloning and Functional Characterization of Psoralen Synthase, the First Committed Monooxygenase of Furanocoumarin Biosynthesis. *J. Biol. Chem.* **2007**, *282*, 542−554.
(48) Adisen, E.; Karaca, F.; Oztas, M.; Gurer, M. A. Efficacy of Local Psoralen Ultraviolet a Treatments in Psoriasis, Vitiligo and Eczema. *Clin. Exp. Dermatol.* **2008**, *33*, 344−345.
(49) Sarker, S. D.; Nahar, L. Natural Medicine:The Genus *Angelica*. *Curr. Med. Chem.* **2004**, *11*, 1479−1500.
(50) Musa, M. A.; Cooperwood, J. S.; Khan, M. O. A Review of Coumarin Derivatives in Pharmacotherapy of Breast Cancer. *Curr. Med. Chem.* **2008**, *15*, 2664−2679.
(51) Lin, Y. H.; Sun, X. X.; Yuan, Q. P.; Yan, Y. J. Combinatorial Biosynthesis of Plant-Specific Coumarins in Bacteria. *Metab. Eng.* **2013**, *18*, 69−77.
(52) Lin, Y.; Shen, X.; Yuan, Q.; Yan, Y. Microbial Biosynthesis of the Anticoagulant Precursor 4-Hydroxycoumarin. *Nat. Commun.* **2013**, *4*, 2603.
(53) Shen, X. L.; Mahajani, M.; Wang, J.; Yang, Y. P.; Yuan, Q. P.; Yan, Y. J.; Lin, Y. H. Elevating 4-Hydroxycoumarin Production through Alleviating Thioesterase-Mediated Salicoyl-CoA Degradation. *Metab. Eng.* **2017**, *42*, 59−65.
(54) Li, S.; Li, Y.; Smolke, C. D. Strategies for Microbial Synthesis of High-Value Phytochemicals. *Nat. Chem.* **2018**, *10*, 395−404.
(55) Currin, A.; Dunstan, M. S.; Johannissen, L. O.; Hollywood, K. A.; Vinaixa, M.; Jervis, A. J.; Swainston, N.; Rattray, N. J. W.; Gardiner, J. M.; Kell, D. B.; Takano, E.; Toogood, H. S.; Scrutton, N. S. Engineering the "Missing Link" in Biosynthetic (−)-Menthol Production: Bacterial Isopulegone Isomerase. *ACS Catal.* **2018**, *8*, 2012−2020.
(56) Nakagawa, A.; Minami, H.; Kim, J. S.; Koyanagi, T.; Katayama, T.; Sato, F.; Kumagai, H. A Bacterial Platform for Fermentative Production of Plant Alkaloids. *Nat. Commun.* **2011**, *2*, 326.

DOI: 10.1021/acscatal.9b01034
ACS Catal. 2019, 9, 5391−5399